http://dx.doi.org/10.5012/bkcs.2014.35.7.1979

Synthesis and Characterization of Graphene and Graphene Oxide Based Palladium Nanocomposites and Their Catalytic Applications in Carbon-Carbon Cross-Coupling Reactions

Minjae Lee, Bo-Hyun Kim,[†] Yuna Lee,[‡] Beom-Tae Kim,[‡,§] and Joon B. Park[†,‡,*]

Department of Chemistry, Kunsan National University, Gunsan 573-701, Korea
[†]Department of Chemistry Education and Institute of Fusion Science, Chonbuk National University, Jeonju 561-756, Korea
[*]E-mail: joonbumpark@jbnu.ac.kr
[‡]Department of Bioactive Material Sciences and Research Center of Bioactive Materials, Chonbuk National University, Jeonju 561-756, Korea
[§]Institute of Basic Liberal Arts Education, Chonbuk National University, Jeonju 561-756, Korea
Received February 19, 2014, Accepted March 7, 2014

We have developed an efficient method to generate highly active Pd and PdO nanoparticles (NPs) dispersed on graphene and graphene oxide (GO) by an impregnation method combined with thermal treatments in H_2 and O_2 gas flows, respectively. The Pd NPs supported on graphene (Pd/G) and the PdO NPs supported on GO (PdO/GO) demonstrated excellent carbon-carbon cross-coupling reactions under a solvent-free, environmentally-friendly condition. The morphological and chemical structures of PdO/GO and Pd/G were fully characterized using X-ray diffraction (XRD), X-ray photoelectron spectroscopy (XPS), and transmission electron microscopy (TEM). We found that the remarkable reactivity of the Pd/G and PdO/GO catalysts toward the cross-coupling reaction is attributed to the high degree of dispersion of the Pd and PdO NPs while the oxidative states of Pd and the oxygen functionalities of graphene oxide are not critical for their catalytic performance.

Key Words : Graphene, Palladium, C-C Cross-coupling reaction, XPS

Introduction

Graphene has attracted increasing attention due to its extraordinary electronic, mechanical, and thermal properties, and has motivated the development of new materials for supercapacity, energy production and conversion, molecular electronics and other related devices.[1-4]

In addition, two-dimensional (2D) sheet of graphene with an extremely high surface-to-volume ratio has great potential, especially as 2D supports for hosting metal nanoparticles (NPs) in heterogeneous catalysis, fuel cells, chemical sensors, and hydrogen storage applications.[5-9]

One of the catalytic applications with the graphene supported metal NPs is the area of carbon-carbon (C-C) and carbon-nitrogen (C-N) cross-coupling reactions.[9-11]

Palladium (Pd) catalyzed C-C and C-N coupling reactions have been of strategic importance since they offer fast reaction rates, high turnover frequency, good selectivity, and high production yield in various synthetic protocols.[12,13]

Recently, several research groups have reported that graphene based palladium catalysts possess good activity and selectivity for various C-C coupling reactions.[14-18]

However, there have been discrepancies in the characterization of the catalytic performance of graphene-based palladium catalysts. For example, Li *et al.* demonstrated that the catalytic activity is strongly influenced by the size distribution of the Pd NPs on graphene sheets, concluding that an even distribution of small Pd NPs is critical for high catalytic performance.[15]

However, it has been claimed that Pd NPs are stable on oxidized graphene sheets and the first layer of the Pd NPs is mainly present as PdO_x. This implies that residual oxygen functionalities on the surface of graphene are critical for stabilizing the Pd NPs and catalytic efficiency.[16]

On the other hand, some studies demonstrated that the oxidative states of Pd NPs play an important role in the catalytic activity, and highly dispersed Pd(0) NPs on graphene sheets are required for high catalytic performance.[17,19]

To clarify these conflicting explanations regarding the performance of the Pd catalysts, we have synthesized graphene and graphene oxide (GO) supported Pd catalysts through an impregnation method combined with thermal treatments. We have evaluated their catalytic performance in C-C cross-coupling reactions. Concurrently, we have characterized their morphological and electronic structures in order to understand how the size distribution and oxidative states of the Pd NPs affect the catalytic efficiency using X-ray diffraction (XRD), X-ray photoelectron spectroscopy (XPS), and transmission electron microscopy (TEM). Here, we demonstrate that the Pd and PdO NPs can be well dispersed on graphene and GO, respectively, and that these NPs act as efficient catalysts in the C-C coupling reactions. We found that the oxidation states of Pd and graphene did not significantly influence the catalytic performance. However, the dispersion and size distribution of the Pd and PdO NPs are critical for high catalytic efficiency.

Experimental

Synthesis of Pd/G and PdO/GO. Graphene oxide (GO) was prepared by the oxidation of graphite powder with H_2SO_4/$KMnO_4$, according to the method of Hummers and Offeman.[20]

Briefly, graphite (2.0 g) was added to concentrated H_2SO_4 (50 mL) in an ice bath, and $NaNO_3$ (1.0 g) and $KMnO_4$ (7.0 g) were slowly added under continuous stirring. After 2 h, the suspension was removed from the ice bath and warmed to 35 °C. The whole reaction mixture was carefully poured into a 5 L flask in an ice bath and H_2O_2 (30%) was added until gas was no longer detected. Then, the suspension was filtered and washed with a 0.1 M HCl solution and distilled water, and then centrifuged at 3,000 rpm. The final product (graphene oxide) was freeze-dried and stored in a vacuum desiccator until further use.

Pd NPs dispersed on graphene (Pd/G) and PdO NPs on graphene oxide (PdO/GO) were prepared through an impregnation method combined with thermal treatments with H_2 and O_2 gases, respectively. Typically, GO (0.9 g) was mixed with $Pd(OAc)_2$ (0.21 g) in 90 mL of distilled water, yielding a homogenous, dark yellow. The resulting suspension was sonicated for 5 min and stirred for 24 h to promote the intercalation of Pd^{2+} on the GO surface. The suspension was filtered and washed with distilled water several times. The filtrate was centrifuged at 3000 rpm and freeze-dried, yielding Pd^{2+} dispersed on GO (Pd^{2+}/GO). The thermal treatment of Pd^{2+}/GO was carried out using a home-built gas flow reactor equipped with gas flow controller (Cole-Parmer), quartz tube, and tubular furnace. The Pd^{2+}/GO was collected in the quartz tube and placed inside the tubular furnace. The furnace was sealed at both ends with end couplings to provide gas flow. The furnace was flashed with Ar gas (100 sccm) for 10 min in advance, and H_2 gas (40 sccm) and O_2 gas (100 sccm) flowed to prepare Pd/G and PdO/GO, respectively. At the same time, the temperature was raised ranging from 100 °C to 500 °C, and maintained for 2 h. The final products were stored in vacuum desiccators before use. Inductively coupled plasma equipped with mass spectrometry (ICP-MS) was utilized to quantify the actual amount of metal loaded on the graphene support.

Characterization of Pd/G and PdO/GO. Powder XRD analyses were performed on a multi-purpose high performance X-ray diffractometer (PANalytical). The diffraction data were recorded for 2θ angles between 6.0° and 80°. XPS spectra were acquired using Mg K_α ($h\nu$ = 1253.6 eV) radiation (KRATOS, AXIS Nova). TEM measurements were performed using a JEM-2200FS. Sonogashira reactions were performed using a microwave reactor (Discover system, CEM).

General Procedure for the C-C Cross-Coupling Reaction. High purity graphite powder (99.99%) and palladium acetate ($Pd(OAc)_2$, 99.99%) were purchased from Sigma-Aldrich and used as received. Iodobenzene, iodobenzene derivatives, phenylacetylene, and 1,8-diazabycyclo[5.4.0] undec7-ene (DBU) were obtained from Sigma-Aldrich. For C-C cross-coupling reactions, phenylacetylene (2 mmol), iodobenzene (1 mmol), DBU (2 mmol), and Pd/G or PdO/GO (1 mol %) were placed in a 5 mL microwave reaction flask. The flask was heated at 120 °C with 300 W in a CEM microwave reactor for 40 min. After cooling to RT, the proceeding of the reaction was monitored by TLC. After removing the catalyst by centrifuge, the reaction product was purified by silica gel column chromatography using hexane as an eluent. After separation, the solvent was evaporated and the product yield was calculated.

Results and Discussion

Preparation and Characterization of Pd/G and PdO/GO. Figure 1(a) and (b) show the typical TEM images of PdO NPs on graphene oxide (PdO/GO) and Pd NPs on graphene (Pd/G), respectively. The PdO/GO and Pd/G were prepared *via* thermal treatments of the Pd precursor impregnated GO (Pd^{2+}/GO) in O_2 and H_2 environments at 100 °C, respectively. It can be seen that the closely anchored NPs are pretty well dispersed without obvious agglomerations on both the GO and graphene surfaces. When more than 50 NPs were randomly chosen and the size distribution was obtained to achieve the desired statistical significance, the average diameters of the NPs of PdO/GO and Pd/G were measured to be 5.6 ± 1.8 nm and 3.4 ± 0.8 nm, respectively. It has been reported that PdO NPs grown on GO are usually larger than Pd NPs on graphene where the average size of the PdO NPs ranged from 4 nm to 15 nm.[17]

The PdO NPs grown on GO are usually oxidized and strongly aggregated by combining the surface oxygen functionalities on the GO surface.

To understand the structural properties of PdO/GO and Pd/G, XRD measurements were performed, as shown in Figure 2(a). The typical diffraction peak (002) of graphene was observed at 2θ = 24.8°, corresponding to a d-spacing of 3.7 Å. A small peak observed at 2θ = 42.6° is associated with the (100) plane of the hexagonal structure of carbon. The peak at 2θ = 40.1° is characteristic of Pd(111) with a face centered cubic structure, and the other peaks exhibit the Pd(200) and Pd(220) planes, suggesting that the Pd is composed of crystalline nanostructures on the graphene surface. When the XRD peaks for PdO/GO were collected, the peaks for graphene were shifted to 2θ = 10.9° due to the presence of various oxygen functional groups in the AB-stacked graphite sheets.

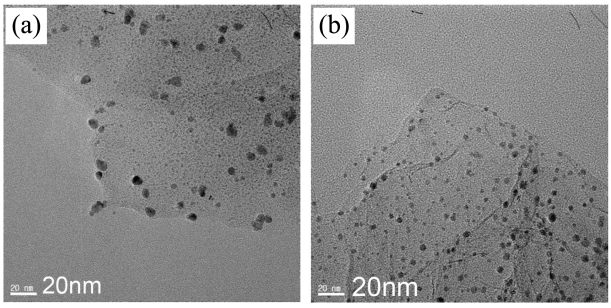

Figure 1. TEM images of (a) PdO/GO and (b) Pd/G.

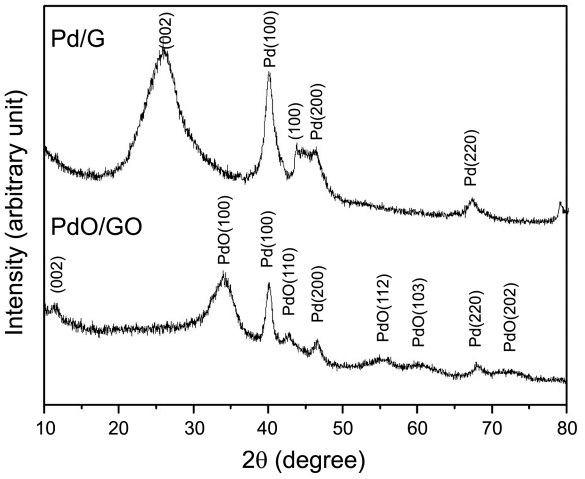

Figure 2. XRD patterns of PdO/GO and Pd/G.

The diffraction peaks for the (100), (110), (112), (103), and (202) planes of crystalline PdO were observed, suggesting that orthorhombic PdO structures are adequately prepared. In addition, small Pd peaks were observed. This indicates that the Pd precursors (Pd^{2+}) were partially converted into the Pd crystalline phase after annealing in O_2 flow at 100 °C. We found that completely oxidized PdO NPs could be obtained above 500 °C. However, this high temperature oxidation resulted in heavily agglomerated PdO NPs, which are not appropriate for our catalytic applications since the larger NPs will deactivate the catalytic performance.

We examined the detailed electronic configurations of PdO/GO and Pd/G using XPS measurements. The Pd 3d XPS results of PdO/GO showed that two symmetrical peaks at 343.1 eV and at 337.8 eV correspond to Pd $3d_{5/2}$ and Pd $3d_{3/2}$, respectively, which suggests that the oxidative state of Pd in PdO/GO is +2 (Figure 3(a)). We can also see a tiny low binding energy peak for the partially reduced Pd (as indicated by arrows), which is pretty consistent with XRD data. The XPS spectrum of Pd/G in the Pd 3d region shows two peaks of Pd $3d_{5/2}$ and Pd $3d_{3/2}$ at 341.2 eV and at 335.9 eV, respectively. These peak positions indicate that the as-prepared Pd NPs on graphene are characteristic of Pd (0). However, the peak shapes appear to be asymmetric on the high binding energy side in both the Pd $3d_{3/2}$ and $3d_{5/2}$ peaks, indicating that the Pd NPs are partially oxidized.

When the XPS spectrum from PdO/GO was collected in the C 1s region, two dominant peaks were observed at 284.7 eV and 286.8 eV, as shown in Figure 3(b). The peak at 284.7 eV is a characteristic peak for the C-C bonding of graphene. The other peak at 286.8 eV is attributed to emissions from a variety of oxygen functional groups (C-OH, -O-, and O=C-OH) on the GO, which indicates that the graphene is almost fully oxidized into GO. Meanwhile, the C1s peak of Pd/G has a maximum at 284.7 eV and the high binding energy peak corresponding to the oxygen functionalities has disappeared. However, a broad tail toward the high binding energy (indicated by arrow) was observed, which implies that the graphene is still partially oxidized after annealing in

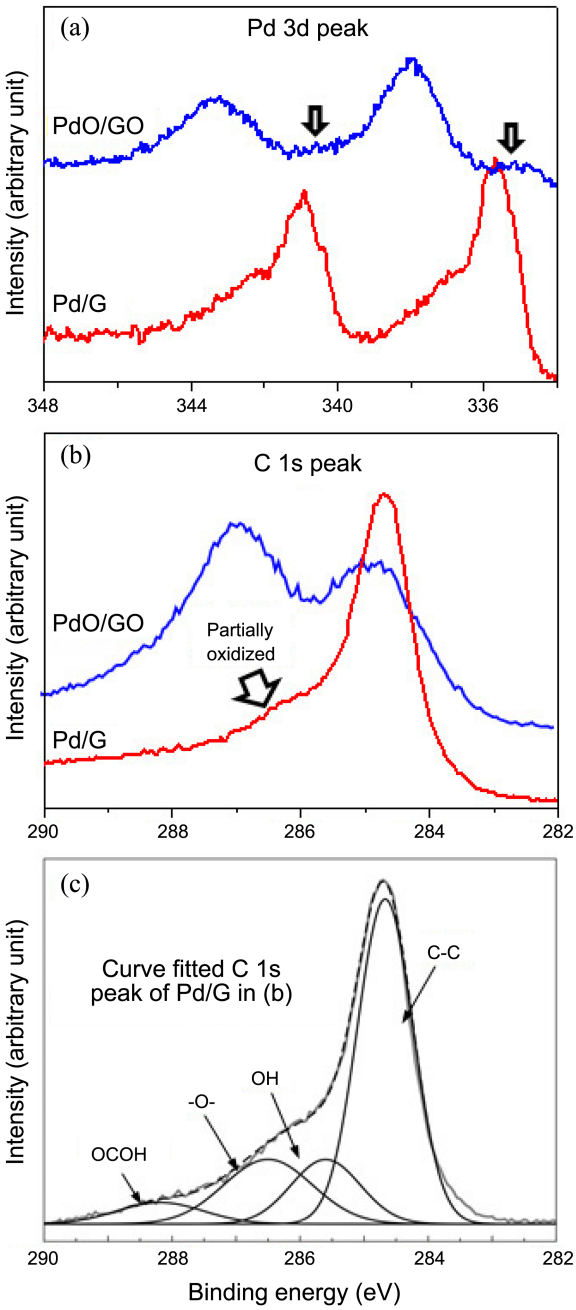

Figure 3. (a) Pd 3d XPS spectra of PdO/GO and Pd/G (100 °C). (b) C 1s XPS spectra of PdO/GO and Pd/G (100 °C). (c) Curve fitted C 1s XPS spectrum of Pd/G.

H_2 flow at 100 °C. When curve fitting of Pd/G (100 °C) was performed using a Gaussian-Lorentzian peak shape (after performing a Shirley background correction), three components were needed to deconvolute the high binding energy shoulder (Figure 4(c)). They occur at 285.6 eV, 286.5 eV, and 288.4 eV and correspond to C-OH, -O-, and O=C-OH, respectively. The curve-fitting results show that about the 24% of carbons in graphene are binding with or influenced by the oxygen functionalities in the normalized area.

In order to prepare highly reduced Pd NPs on graphene for catalytic applications, we heated the Pd^{2+}/GO at higher temperature ranging from 200 °C to 500 °C in H_2 flow and

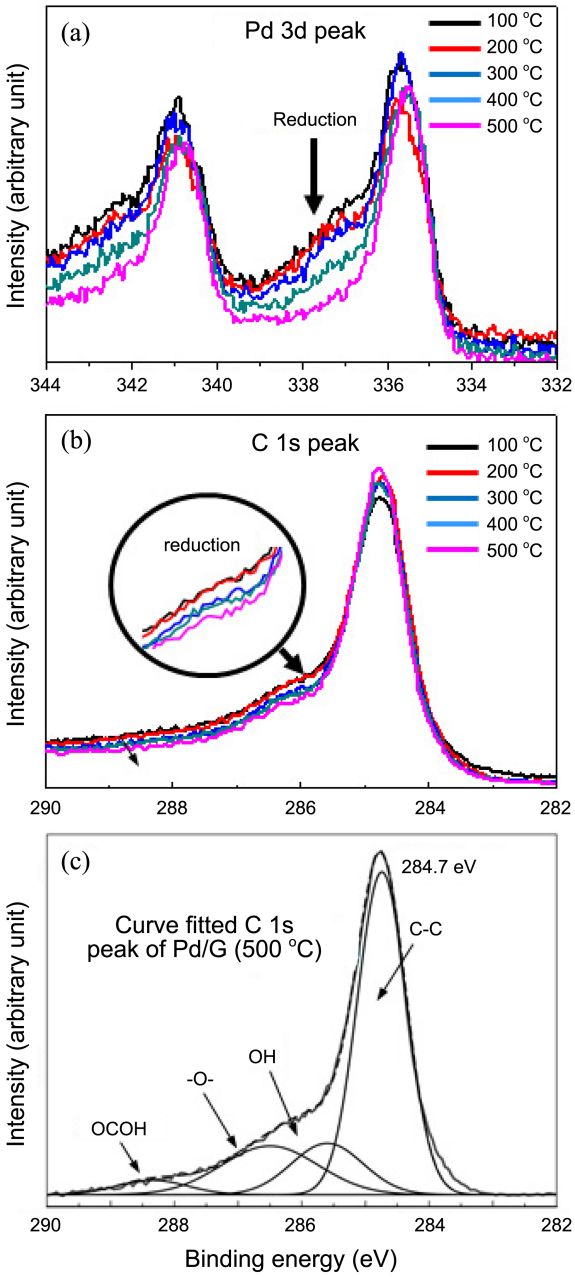

Figure 4. (a) Pd 3d and (b) C 1s XPS spectra of Pd/G. The Pd/G was prepared by heating Pd^{2+}/GO in an H_2 environment from 100 °C to 500 °C. (c) Curve fitted C 1s XPS spectrum of Pd/G (500 °C).

analyzed the NPs with XPS and TEM. As the annealing temperature increased, the high binding energy shoulders of Pd $3d_{5/2}$ and Pd $3d_{3/2}$ corresponding to the oxidized Pd NPs decreased. Peak shapes also changed and became fairly symmetric after annealing at 500 °C, as shown in Figure 4(a). When C 1s XPS spectra for the reduced Pd/G were collected, the high binding energy shoulders also decreased with the annealing temperature (Figure 4(b)). The curve-fitted results of the C 1s peak after heating at 500 °C show that the peak area corresponding to high binding energy shoulder is calculated to be 19% in the normalized area. This means that approximately 21% of the oxygen functionalities were converted to the characteristic C-C bonds after heating at 500

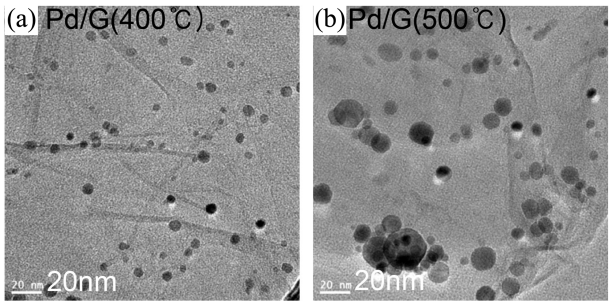

Figure 5. TEM images of (a) Pd/G (400 °C) and (b) Pd/G (500 °C).

°C. Nonetheless, these annealing conditions could not generate completely reduced graphene layers. It has been reported that rapid heating to higher than 1000 °C is required to completely convert GO into reduced graphene.[21]

Morphological changes of the highly reduced Pd/G have been characterized by TEM. Figure 5(a) and (b) show the TEM images of Pd/G annealed at 400 °C and 500 °C, respectively. It can be seen that the degree of agglomeration of the Pd NPs on the graphene surface is significantly higher compared with Pd/G at 100 °C, as observed in Figure 1(b). The average diameters of the Pd NPs of Pd/G at 400 °C and 500 °C were measured to be 11.3 ± 3.6 nm and 23.6 ± 6.8 nm, respectively.

Based on the XPS and TEM results, we can explain how the electronic and morphological properties of Pd/G change with annealing temperature. The as-prepared Pd/G at 100 °C in H_2 flow is composed of partially oxidized Pd NPs and graphene. The small NPs with an average diameter of 3.4 nm are evenly dispersed without obvious agglomerations on the surface of the graphene. As the heating temperature increases, graphene becomes more reduced and the Pd NPs are sintered and grow larger. The agglomeration of Pd NPs at higher temperatures can be explained by an Ostwald ripening process, which is a mechanism of cluster growth on the supporting materials. When oxide supported NPs are placed in a high temperature environment, there is detachment of surface atoms from the smaller NPs, followed by reattachment of those atoms to the more stable surfaces of the larger NPs. As a result of Ostwald ripening, the number of density of Pd NPs on graphene decreased and the average

Table 1. Catalytic yields of the Sonogashira reaction of PdO/GO and Pd/G

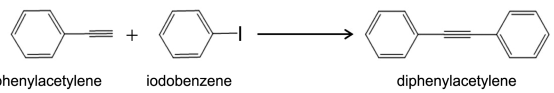

Catalyst	Pd/D					PdO/GO
Temp.[a]	100 °C	200 °C	300 °C	400 °C	500 °C	100 °C
Yield[b]	95	95	92	61	22	92

Reaction condition: aryl iodide (1.0 mmol), alkyne (2.0 mmol), Pd/graphene (1 mol %), DBU (2.0 mmol). Microwave reactor system (300W, 120 °C, CEM Discover model,) was used. [a]calcination temperature to prepare Pd/G and PdO/GO. [b]Isolated yields.

size of Pd NPs increased from 3.4 ± 0.6 nm (at 100 °C) to 23.6 ± 6.8 nm (at 500 °C).

Catalytic Activity of PdO/GO, Pd/G and Reduced Pd/G. The Sonogashira reaction is one of the most widely used synthetic protocols for carbon-carbon or carbon-heteroatom bond formations. Especially, microwave-assisted solvent-free Sonogashira reactions have been demonstrated to be an effective approach in organic synthesis because the maximization of substrate loadings, increased selectivity, toxic solvent-free condition, and easy separation for recycling are possible. We investigated the catalytic activities of Pd/G and PdO/GO (treated H_2 or O_2 at 100-500 °C) in the formation of diphenylacetylene using the Sonogashira reaction of iodobenzene and phenylacetylene (Table 1). When Pd/G (100 °C) was used, the reaction yield reached as high as 95%. This implies that the Pd/G can act as an efficient catalyst in the microwave-assisted solvent-free condition. In case of the PdO/GO, the yield reached 92%. The difference between these two yields is negligible within experimental error. These results imply that the oxidative states of Pd NPs and graphene do not significantly influence the catalytic efficiency. When highly reduced Pd/G (200-500 °C) was used as catalysts, the reaction yield decreased with the annealing temperature. The reaction yield remained fairly consistent up to 300 °C, but it dropped at 400 °C and again at 500 °C, showing 61% and 22%, respectively. The deactivation of the Pd/G catalyst can be explained from Figure 5, which shows TEM images of sintered and agglomerated Pd NPs. This implies that the size and distribution of Pd NPs on graphene could be key factors for catalytic activity in this reaction. Generally, the highly dispersed metal NPs on supports with smaller diameters are known to have higher catalytic activity due to the advantages of increased low coordination numbers in metal NPs and larger surface area; these imply higher number of active sites.[22,23] The size-dependent electronic structural change may also contribute to increased catalytic efficiency.[24,25]

To generalize the above results, three other iodobenzene derivatives were used for the preparation of diphenylacetylene derivatives in the same reaction condition. For these experiments, we chose to use the Pd/G (100 °C) exclusively due to the higher catalytic activity demonstrated. As illustrated in Table 2, the reactions proceeded fairly well with other aryl iodides containing electron donating groups.

Table 2. Sonogashira reactions of different iodoben-zene with Pd/G

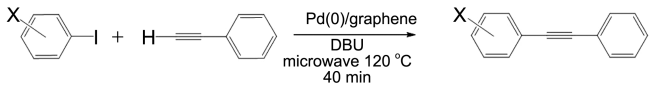

Entry	RX	Product	Yield (%)[b]
1		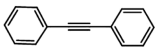	95
2	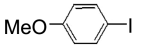	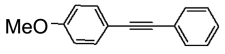	92
3		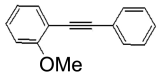	90
4	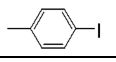	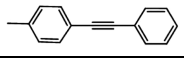	99

Conclusion

In conclusion, we have developed an efficient method to generate highly active Pd and PdO NPs on graphene and GO through an impregnation method combined with thermal treatments. Both Pd/G and PdO/GO demonstrated excellent catalytic activities for carbon-carbon cross-coupling reactions under solvent-free environmentally-friendly conditions. We found strong evidence that the outstanding catalytic activity toward the Sonogashira reaction is associated with even distribution of small Pd or PdO NPs on graphene surface. The oxidative states of Pd atoms in Pd NPs and oxygen functionalities of graphene oxide do not appear to critically influence catalytic performance.

Acknowledgments. This research was supported by the Basic Science Research Program through the National Research Foundation of Korea (NRF), funded by the Ministry of Education Science and Technology (No. 2011-0011880). This paper also includes research that was accomplished as "Industry-University-Research Institute Core Technology Development & Industrialized Supporting Business" supported by Chonbuk province in 2013 (2013C14).

References

1. Wu, Z. S.; Ren, W. C.; Wen, L.; Gao, L. B.; Zhao, J. P.; Chen, Z. P.; Zhou, G. M.; Li, F.; Cheng, H. M. *ACS Nano* **2010**, *4*, 3187.
2. Kamat, P. V. *J. Phys. Chem. Lett.* **2010**, *1*, 520.
3. Khalid, N. R.; Hong, Z. L.; Ahmed, E.; Zhang, Y. W.; Chan, H.; Ahmad, M. *Appl. Surf. Sci.* **2012**, *258*, 5827.
4. Chen, S.; Zhu, J. W.; Wu, X. D.; Han, Q. F.; Wang, X. *ACS Nano* **2010**, *4*, 2822.
5. Sun, Y. M.; Hu, X. L.; Luo, W.; Xia, F. F.; Huang, Y. H. *Adv. Funct. Mater.* **2013**, *23*, 2436.
6. Hsieh, C. T.; Lin, C. Y.; Lin, J. Y. *Electrochim. Acta* **2011**, *56*, 8861.
7. Chen, X. M.; Wu, G. H.; Chen, J. M.; Chen, X.; Xie, Z. X.; Wang, X. R. *J. Am. Chem. Soc.* **2011**, *133*, 3693.
8. Parambhath, V. B.; Nagar, R.; Sethupathi, K.; Ramaprabhu, S. *J. Phys. Chem. C* **2011**, *115*, 15679.
9. Djakovitch, L.; Kohler, K. *J. Organomet. Chem.* **2000**, *606*, 101.
10. Xu, C.; Wang, X.; Zhu, J. W. *J. Phys. Chem. C* **2008**, *112*, 19841.
11. Yi, C. Y.; Hua, R. M. *Catal. Commun.* **2006**, *7*, 377.
12. Ramakrishnan, A.; Dumbuya, K.; Ofili, J.; Steinruck, H. P.; Gottfried, J. M.; Schwieger, W. *Appl. Clay Sci.* **2011**, *51*, 8.
13. Djakovitch, L.; Koehler, K. *J. Am. Chem. Soc.* **2001**, *123*, 5990.
14. Scheuermann, G. M.; Rumi, L.; Steurer, P.; Bannwarth, W.; Mulhaupt, R. *J. Am. Chem. Soc.* **2009**, *131*, 8262.
15. Li, Y.; Fan, X. B.; Qi, J. J.; Ji, J. Y.; Wang, S. L.; Zhang, G. L.; Zhang, F. B. *Nano Res.* **2010**, *3*, 429.
16. Li, Y. Z.; Yu, Y.; Wang, J. G.; Song, J.; Li, Q.; Dong, M. D.; Liu, C. J. *Appl. Catal. B* **2012**, *125*, 189.
17. Siamaki, A. R.; Khder, A. E. S.; Abdelsayed, V.; El-Shall, M. S.; Gupton, B. F. *J. Catal.* **2011**, *279*, 1.
18. Lee, K. H.; Han, S. W.; Kwon, K. Y.; Park, J. B. *J. Colloid and Interface Sci.* **2013**, *403*, 127.
19. Yan, N.; Xiao, C. X.; Kou, Y. *Coord. Chem. Rev.* **2010**, *254*, 1179.

20. E.Offeman, W. S. H. a. R. *J. Am. Chem. Soc.* **1958**, *80*, 1339.
21. Yang, D.; Velamakanni, A.; Bozoklu, G.; Park, S.; Stoller, M.; Piner, R. D.; Stankovich, S.; Jung, I.; Field, D. A.; Ventrice, C. A.; Ruoff, R. S. *Carbon* **2009**, *47*, 145.
22. Remediakis, I. N.; Lopez, N.; Norskov, J. K. *Angew. Chem. Int. Ed.* **2005**, *44*, 1824.
23. Lopez, N.; Janssens, T. V. W.; Clausen, B. S.; Xu, Y.; Mavrikakis, M.; Bligaard, T.; Norskov, J. K. *J. Catal.* **2004**, *223*, 232.
24. Chen, M. S.; Goodman, D. W. *Science* **2004**, *306*, 252.
25. Santra, A. K.; Yang, F.; Goodman, D. W. *Surf. Sci.* **2004**, *548*, 324.